DISCLAIMER: This preprint should not be cited.

In this manuscript, we report that P granules are stable *ex vivo*. While this main observation is robust and reproducible, we have found that the method we used to mount embryos for laser manipulation interfered with some of the *ex vivo* assays. We therefore ask that this version not be cited. We apologize for any inconvenience this may have caused.

Examination of P granule dynamics *in vivo* and *ex vivo*

Jarrett Smith and Geraldine Seydoux, Dept. of Molecular Biology and Genetics, HHMI, Johns Hopkins University, School of Medicine, 725 N. Wolfe Street, Baltimore MD 21205, USA

Corresponding author: gseydoux@jhmi.edu

ABSTRACT – *This preprint should not be cited*.

RNA granules are RNA/protein condensates proposed to form in cells by liquid-liquid phase separation, a thermodynamic process that partitions molecules between two liquid phases without energy input. The *C. elegans* P granules are RNA granules that exhibit liquid-like behaviors. Using *ex vivo* methods, we find that P granules are not simple liquids. P granules solidify outside of cells, becoming resistant to dilution and high salt. P granules also solidify in cells upon shift to high temperature or inactivation of the DDX6 RNA helicase. Solidification of RNA granules has been linked to neurodegeneration. Our findings suggest that active processes are needed continuously to counteract the intrinsic propensity of RNA granules to solidify.

MAIN TEXT

The P granules of the *C. elegans* germline were the first RNA granules shown to display liquid-like behaviors (Brangwynne, Eckmann et al. 2009). P granules are roughly round, fuse, can be deformed by flows, and their components exchange rapidly with the cytoplasm. Based on these properties, P granules were proposed to assemble by liquid-liquid phase separation (LLPS), a spontaneous de-mixing process that relies on low-affinity interactions to coalesce molecules into a liquid droplet that maintains dynamic exchange with the surrounding cytoplasm

(Hyman, Weber et al. 2014). A role for LLPS in P granule assembly is also supported by experiments showing that purified P granule proteins undergo LLPS *in vitro* (Elbaum-Garfinkle, Kim et al. 2015, Saha, Weber et al. 2016, Smith, Calidas et al. 2016). Similar experiments with proteins from other cellular condensates have suggested that LLPS is a general mechanism underlying the formation of a diverse set of non-membranous cellular organelles (Shin and Brangwynne 2017). Few studies, however, have probed the properties of natural condensates assembled *in vivo*, which can contain dozens of proteins (Updike and Strome 2010, Jain, Wheeler et al. 2016). LLPS requires super-saturated conditions to support continuous diffusion of components in and out of the droplets (Brangwynne, Tompa et al. 2015, Saha, Weber et al. 2016). A shift to an under-saturated environment would be predicted to dissolve liquid condensates. To test this prediction, we used a laser to puncture the eggshell of live *C. elegans* embryos and extrude their contents into aqueous buffer (Fig. 1). We monitored P granules using a line co-expressing a MEG-3::GFP transgene and a mCherry::PGL-3 transgene. The intrinsically-disordered protein MEG-3 is a "scaffold" protein required for granule assembly and the RGG domain protein PGL-3 is a "client" that is recruited to the granules by MEG-3 (Kawasaki, Amiri et al. 2004, Wang, Smith et al. 2014, Smith, Calidas et al. 2016). In intact embryos, MEG-3::GFP and mCherry::PGL-3 exhibit similar rates of granule-cytoplasm exchange, achieving between 70-80% fluorescence recovery 90 seconds after photobleaching (FRAP) of whole granules (Fig. S1A). MEG-3::GFP and mCherry::PGL-3, however, responded differently to extrusion. As expected for a simple liquid phase, mCherry::PGL-3 diffused immediately (< 5 seconds) upon extrusion into aqueous buffer. In contrast, MEG-3::GFP persisted in the granules, as they flowed out of the embryo and into the dilute buffer (Fig. 1A and Movie 1). We obtained the same result using a line expressing MEG-3::GFP from the endogenous *meg-3* locus (Table S1) (Fig. S1D and Fig. 2). Using this line, we quantified the fraction of MEG-3 remaining in the granule phase after extrusion by measuring GFP fluorescence in granules before and after extrusion. We found that on average 76% of MEG-3::GFP (± 0.22 standard deviation) remained in the

granule phase after extrusion (Fig. 1B), compared to 0% for mCherry::PGL-3 (Fig. S1B). The extruded MEG-3::GFP granules persisted in buffer for at least an 1 hour (Fig. S1C). We obtained similar results with the MEG-3 homolog MEG-1 and the PGL-3 homolog PGL-1. MEG-1::GFP remained in granules upon extrusion and PGL-1::GFP diffused immediately upon extrusion (Fig. S1D). We conclude that P granules contain at least two distinct phases: an intrinsically dynamic, liquid PGL phase and an intrinsically more stable MEG phase that requires *in vivo* conditions to remain dynamic. To investigate the nature of the MEG phase, we repeated the extrusion experiments into buffer containing different additives (Fig. 1B). MEG-3::GFP granules were stable in high salt (1M NaCl) and 2,5 hexanediol (5%), but dissolved in SDS (0.5%) and 1,6 hexanediol (5%), an aliphatic alcohol known to dissolve P granules *in vivo* (Updike, Hachey et al. 2011). These results are consistent with a protein-based phase held by hydrophobic interactions.

The stability of the MEG-3 phase *ex vivo* (Fig. 1) contrasts with the rapid dynamics of MEG-3 *in vivo* (Fig. S1A). *In vivo*, many active processes use ATP hydrolysis as a source of energy (Knowles 1980). We reasoned that if MEG-3 dynamics are ATP-driven, it may be possible to restore liquid-like behavior to MEG-3 granules *ex vivo* by providing exogenous ATP. Therefore, we repeated the extrusion experiments using buffer supplemented with various concentrations of ATP coordinated with Mg^{2+} (ATP*Mg), the form of ATP used by most enzymes (Mildvan 1987). We found that 7mM ATP was sufficient to completely dissolve MEG-3 granules within 60 seconds after extrusion (Fig. 2, Movie 2, and Fig. S2A). Dissolution was sensitive to pH, with maximal activity at pH 6.5 and lower (Fig. S2B). *In vitro*, ATP has been reported to dissolve protein condensates by acting as a hydrotrope, a molecule with hydrophilic and hydrophobic moieties capable of solubilizing hydrophobic compounds in aqueous solutions. Like ATP, GTP and non-hydrolysable ATP analogs also exhibit hydrotrope-like properties *in vitro* (Patel, Malinovska et al. 2017). In contrast, we found that GTP, ADPnP, ADP, and AMP had no effect on extruded MEG-3::GFP granules (Fig. 2B, Movie 3). ATP typically requires Mg^{2+} (ATP*Mg) to be used as an energy source by

enzymes (Mildvan 1987). We found that ATP combined with Ca^{2+} (ATP*Ca) did not support efficient MEG-3 dissolution (Fig. 2B). These findings suggest that the liquid-like dynamics of MEG-3 are dependent on active, energy-driven processes that require ATP hydrolysis.

To explore whether MEG-3 dynamics are also energy-dependent in intact embryos, we measured MEG-3 dynamics in embryos raised above the thermal limit. Aerobic respiration becomes impaired in embryos raised above the *C. elegans* upper thermal limit of 26°C, causing energy-requiring processes to slow down or fail (Neves, Busso et al. 2015). Above the thermal limit, MEG-3 dynamics should decrease if dependent on active processes, but should increase if dependent only on thermodynamics. Consistent with the former, we found that MEG-3 granule/cytoplasmic exchange slowed substantially in embryos shifted to 28°C for 40 minutes or to 30°C for 120 minutes. The immobile MEG-3::GFP granule fraction increased from 16% at 20°C , to 48% at 28°C and 75% at 30°C (Fig. 3A). Conversely, we found that the PGL-3 granule phase was reduced at high temperatures. In embryos co-expressing MEG-3::GFP and mCherry::PGL-3, 93% (n=45) of MEG-3::GFP granules were positive for mCherry::PGL-3 at 20°C, but only 60% (n=47) after 40 minutes at 28°C and 14% (n=64) after 120 minutes at 30°C. PGL-1 has also been reported to undergo reversible dissolution in response to high temperature (Delgadillo 2016). We conclude that P granules contain both a thermodynamic liquid PGL phase that dissolves in response to high temperature, and an active MEG-3 phase that solidifies at high temperatures, likely due to reduced energy availability (also see below).

ATP-utilizing kinases, chaperones and RNA helicases have all been implicated in driving RNA granule assembly and/or disassembly (Hubstenberger, Noble et al. 2013, Wippich, Bodenmiller et al. 2013, Wang, Smith et al. 2014, Hubstenberger, Cameron et al. 2015, Jain, Wheeler et al. 2016, Mugler, Hondele et al. 2016, Alberti, Mateju et al. 2017). To determine the ATPase responsible for MEG-3 dynamics, we first tested the effect of chemical inhibitors on MEG-3::GFP granule dissolution in the presence of ATP *ex vivo*. Neither staurosporine, a general protein kinase inhibitor, nor 17-AAG, an inhibitor of chaperone HSP90,

prevented P granule dissolution (Fig. S3A). P granules contain several DEAD-box RNA helicases including GLH-1, LAF-1, and CGH-1, the *C. elegans* homologs of the VASA, DDX3, and DDX6 helicases respectively (Updike and Strome 2010, Elbaum-Garfinkle, Kim et al. 2015). To determine whether these helicases contribute to MEG-3 dynamics, we first tested which helicase remained associated with granules upon extrusion. LAF-1::GFP and GLH-1::RFP dissolved immediately upon granule extrusion, as observed with PGL-1 and PGL-3 (Fig. S1D). In contrast, CGH-1::GFP remained in granules *ex vivo* (Fig. S1D). CGH-1/DDX6 is a RNA helicase involved in many aspects of RNA metabolism (Bourgeois, Mortreux et al. 2016). CGH-1/DDX6 homologs have already been implicated in the regulation of RNA granule dynamics in *C. elegans* oocytes (Hubstenberger, Noble et al. 2013, Hubstenberger, Cameron et al. 2015) and yeast (Mugler, Hondele et al. 2016). *cgh-1(null)* mutants are sterile and produce no embryos. To examine the function of CGH-1 in embryos, we used *cgh-1(tn691)*, a temperature-sensitive *(ts)* mutation in the ATP-binding domain of CGH-1 (Hubstenberger, Noble et al. 2013). We crossed the *cgh-1(tn691)* allele into our MEG-3::GFP line and refer to this line hereafter as *cgh-1(ts)* (Table S1). When grown at 20°C, *cgh-1(ts)* hermaphrodites are fertile and generate viable embryos. We found that, when shifted to the non-permissive temperature of 25°C for 120 minutes, *cgh-1(ts)* embryos accumulated ectopic P granules in the anterior cytoplasm which normally does not support granule formation (Fig. S3B). FRAP analyses of MEG-3::GFP in *cgh-1(ts)* embryos revealed severely impaired MEG-3 dynamics, with a granule immobile fraction larger than 80% (Figure 3B). This reduction in MEG-3 dynamics was not observed in wild-type embryos raised at 25°C (Figure 3B), but was similar to that observed in wild-type embryos shifted above the thermal limit (>26°C, Fig. 3A). In the latter, the slower dynamics were due, presumably, to a reduction in endogenous ATP, whereas the slower dynamics of *cgh-1(ts)* granules were due presumably to reduced helicase activity. Consistent with this hypothesis, we found that granules extruded from wild-type embryos raised at 28°C quickly dissolved in egg buffer supplemented with ATP (Fig. 3C). In contrast, granules extruded from *cgh-1(ts)* embryos raised

at 25°C were resistant to dissolution by ATP (Fig. 3D and Fig. S3B). We conclude that CGH-1/DDX6 is one of the ATP-consuming enzymes that contributes to the liquid-like dynamics of the MEG-3 phase. How CGH-1 affects the MEG-3 phase remains to be determined, but activation of the ATPase activity of Dhh1, the yeast homolog of CGH-1, is sufficient to dissolve Dhh1/RNA droplets *in vitro* (Mugler, Hondele et al. 2016).

Our findings suggest that P granules are complex condensates that contain at least two phases: an energy-consuming (active) phase that contains MEG proteins, and a thermodynamic (passive) phase that contains PGL proteins. The MEG phase is required to stabilize the PGL phase and the two do not mix completely in the granules (Wang, Smith et al. 2014, Smith, Calidas et al. 2016). Under optimal culture conditions, both phases exhibit liquid-like behaviors, with similar rates of granule/cytoplasm exchange (Fig. S1A) and similar dynamics during granule fusion (Wang, Smith et al. 2014). Active and passive liquid-like phases have also been described in nucleoli and stress granules, which also solidify when extruded from cells (Brangwynne, Mitchison et al. 2011, Jain, Wheeler et al. 2016, Falahati and Wieschaus 2017). Active scaffolds may therefore be a common underlying feature of RNA granules. Aberrant solidification of RNA granules, as well as aging and ATP-deprived environments, have been linked to certain neurodegenerative disorders (Taylor, Brown et al. 2016). We suggest that the scaffolds that support RNA granule assembly require continuous ATP consumption to avoid solidification. An interesting corollary is that ATP availability tunes the fluidity of RNA granules even under physiological conditions (Kedersha, Chen et al. 2002, Wurtz and Lee 2017). Cellular ATP concentrations have been estimated to range between 1 to 10mM (Traut 1994). In our hands, rapid dissolution of P granules *ex vivo* requires a relatively high concentration of ATP (7mM; Fig. S2A). We suggest that intermediate ATP levels promote the assembly of transient, liquid-like phases like P granules, while lower ATP levels give rise to non-dynamic granules like the Balbiani body of resting oocytes (Boke, Ruer et al. 2016) or the pathogenic aggregates of aged neurons (Taylor, Brown et al. 2016). Although ATP may function as a hydrotrope in some

contexts (Patel, Malinovska et al. 2017), our findings suggest that ATP-consumption by enzymes, such as the RNA helicase DDX6, is essential to maintain RNA granules in a liquid-like state in cells. In this respect, RNA granules may be similar to other self-organizing, polymer networks (e.g. actin cytoskeleton) that use energy to generate liquid-like behaviors (Humphrey, Duggan et al. 2002, Needleman and Brugues 2014) and models that only consider equilibrium dynamics may not be sufficient to describe the properties of RNA granules in cells.

Acknowledgments:

We thank Dominique Rasoloson who provided strains JH3269 and JH3379. Some strains were provided by the CGC, which is funded by NIH Office of Research Infrastructure Programs (P40 OD010440). This work was supported by the National Institutes of Health (NIH) (grant number R37 HD37047). G.S. is an investigator of the Howard Hughes Medical Institute.

Materials and Methods

Strains Used – C. elegans was cultured according to standard methods (Brenner 1974) at 20°C unless otherwise stated. Strains used in this study are listed in Table S1.

Chemicals Used – Adenosine 5'-triphosphate disodium salt hydrate – ATP (A2383, Sigma), Adenosine 5'-diphosphate sodium salt - ADP (A2754, Sigma), Adenosine 5'-monophosphate disodium - AMP (01930, Sigma), Adenosine 5'-(β,γ-imido)triphosphate lithium salt hydrate – ADPnP (A2647, Sigma), Guanosine 5'-triphosphate sodium salt – GTP (G8877, Sigma), Magnesium Chloride – $MgCl_2$ (M8266, Sigma), Ethylenediaminetetraacetic acid disodium salt dihydrate – EDTA (ED2SS, Sigma), Sodium Chloride – NaCl (S9888, Sigma), 1, 6 Hexanediol (240117, Sigma), 2, 5 Hexanediol (H11904, Sigma), Sodium dodecyl sulfate – SDS (L3771, Sigma), Dimethyl sulfoxide – DMSO (276855, Sigma), Staurosporine (A8192, ApexBio), 17-AAG (KOS953) (A4054, ApexBio).

Preparation of ATP analogue Extrusion Buffers – All ATP and ATP analogue stock solutions were prepared in egg buffer (83 mM NaCl, 33 mM KCl, 1.5 mM $CaCl_2$, 7.5mM $MgCl_2$, 50 mM Hepes pH 6.5). Unless otherwise indicated, solutions were buffered to pH 6.5 with NaOH and HCl using a Mettler Toledo Seveneasy pH meter and a Fisherbrand™ Accumet™ glass body standard combination mercury free electrode.

Confocal Microscopy - Fluorescence microscopy was performed using a Zeiss Axio Imager with a Yokogawa spinning-disc confocal scanner. Photomicrographs were taken using Slidebook v 6.0 software (Intelligent Imaging Innovations). For live imaging of extruded granules, embryos were dissected from adult hermaphrodites in egg buffer salt solution (83 mM NaCl, 33 mM KCl, 1.5 mM $CaCl_2$, 7.5mM $MgCl_2$, 50 mM Hepes) and mounted on glass slides with egg buffer. Embryo contents were extruded by ablating the eggshell using a 3i Ablate!™ laser system at 532 nm pulse setting with a power level of 155 and 10 cycles. All embryo images are z stack maximum projections using a z step size of 1µm, spanning the entire depth of the embryo. Images were acquired using 25ms exposures in the 488 channel or 50ms exposures in the 561 channel continuously using a 63x objective.

Quantification of MEG-3::GFP and mCherry::PGL-3 after extrusion – For MEG-3::GFP, photomicrographs acquired as described above were analyzed using Image J64. Background was subtracted from each image using a rolling ball radius of 15 pixels, a pixel brightness threshold was set to 31-255. Remaining pixels were smoothed 1 time and the total integrated density of the objects (P granules) was quantified. Total fluorescence intensity was calculated before (I_B) and after (I_A) extrusion and used to calculate a fluorescence ratio (I_A /I_B). For some embryos, granules left the field of view and could not be counted. The I_A /I_B, therefore, is a minimal estimate of the fraction of MEG-3 that remains in the granule phase after extrusion. mCherry::PGL-3 images were analyzed and quantified similarly using a pixel brightness threshold of 40-255.

Fluorescence Recovery after Photobleaching (FRAP) - All FRAP imaging was performed using a Zeiss LSM 800 GaAsp system. Embryos were dissected

from adult hermaphrodites in M9 salt solution and mounted onto 3% agarose on glass slides. Experiments were performed by imaging at 5% laser power in the 488 or 561 channels with a gain of 700 and bleaching was performed using an area slightly larger than the granules (~2.5 μM diameter) using 50% laser power in the 488 and 561 channels (for GFP and mCherry respectively). Single slice images were taken every second during a recovery phase of >90 seconds. The mean fluorescence intensity of the area containing the granule was measured at each time point using ImageJ/Fiji. At each time point, the fluorescence intensity from the FRAPed granule (G_i) was normalized to the fluorescence intensity of the unFRAPed cytoplasm (C_i) to account for bleaching due to imaging. G_i/C_i at each time point was then normalized to the initial time point. The normalized fluorescence recovery was averaged for each time point across multiple independent FRAP experiments (> 8 granules). Average fluorescence intensity was plotted with ± standard error.

Crossing of cgh-1(ts) mutant with MEG-3::GFP strain – Young *cgh-1(tn691)* (DG1701, Table S1) males were mated with MEG-3::GFP L4 hermaphrodites (JH3503). F2 progeny were singled out and screened for MEG-3::GFP expression. The progeny from MEG-3::GFP positive F2 hermaphrodites were screened for homozygous MEG-3::GFP and *cgh-1(tn691)* mutation by PCR and sequencing. Two independent lines were obtained using this method (Table S1). Both lines were utilized in FRAP and extrusion experiments (Fig. 3B and Fig. 3D. JH3546 only was used in Fig. S3B)

Temperature shifts– Young adult worms were shifted to agar plates pre-incubated at the desired temperature in a UVP HB-1000 Hybridizer incubator or an Innova 4230 Refrigerated Incubator. After incubation, embryos were dissected and mounted onto either glass sides (extrusion experiments) or agarose pads on glass sides (FRAP experiments) for immediate analysis.

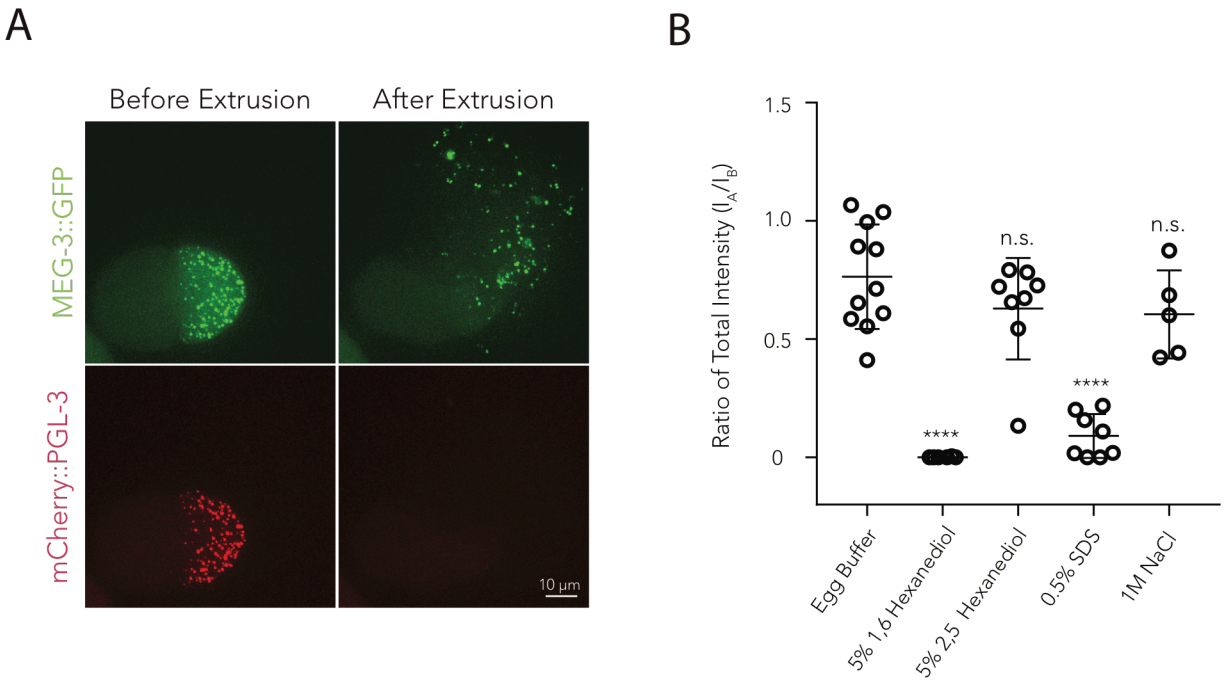

Fig. 1 – The MEG-3 granule phase is stable in aqueous buffer

A. Fluorescent images of a wild-type 2-cell embryo co-expressing transgenes MEG-3::GFP and mCherry::PGL-3 (strain JH3019) before (left) and after (right) laser puncture of the eggshell. Before laser puncture, the P granules, marked by MEG-3::GFP (green) and mCherry::PGL-3 (red), are in the posterior germline blastomere. Laser puncture causes the contents of the posterior blastomere to spill onto the slide mixing with the aqueous buffer. MEG-3::GFP perdures in the granule phase, whereas mCherry::PGL-3 becomes dispersed. Scale bar is 10µm.

B. Graph showing the fraction of MEG-3::GFP retained in the granular phase after extrusion. Data were obtained using strain JH3503 (MEG-3::GFP^{CRISPR}). Total GFP fluorescence from granules was measured before laser puncture (I_B) and 60 seconds after laser puncture (I_A). The I_A /I_B ratio is shown for each embryo (circle) extruded into the indicated buffers. Egg buffer (83 mM NaCl, 33 mM KCl, 1.5 mM $CaCl_2$, 7.5mM $MgCl_2$, 50 mM Hepes pH 7.0) is the base-line buffer to which additives were added. Means are indicated along with error bars representing ± SD. X – axis shows the buffer conditions for each group. P values were computed comparing each condition to buffer alone. n.s indicates that $p > 0.05$, *$p < 0.05$, **$p < 0.01$, ***$p < 0.001$, ****$p < 0.0001$.

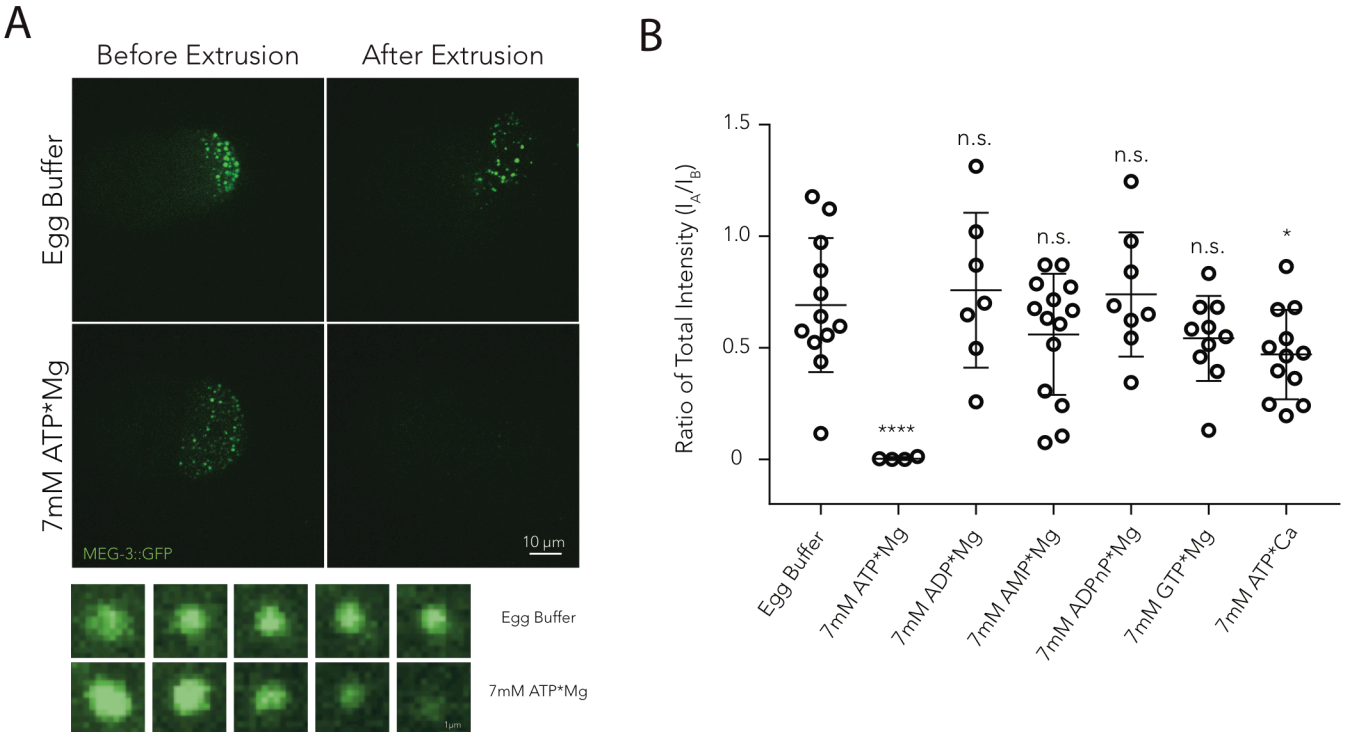

Fig. 2 – ATP dissolves the MEG-3 granule phase

A. (Top) Photomicrographs of wild-type embryos expressing MEG-3::GFP (JH3503) before (left) and after (right) extrusion of P granules into egg buffer or egg buffer containing 7mM ATP*Mg. Scale bar is 10 µm long.

(Bottom) MEG-3::GFP granule dissolution over time. Time-lapse photomicrographs of P granules labeled with MEG-3::GFP (JH3503) before and after extrusion into egg buffer or 7mM ATP*Mg. Time after extrusion is shown below each image. Scale bar is 1µm long.

B. Graph showing the fraction of MEG-3::GFP retained in the granular phase after extrusion. Data were obtained and quantified as in Fig. 1B. See Fig. S2 for effect of pH and ATP concentration on MEG-3 dissolution.

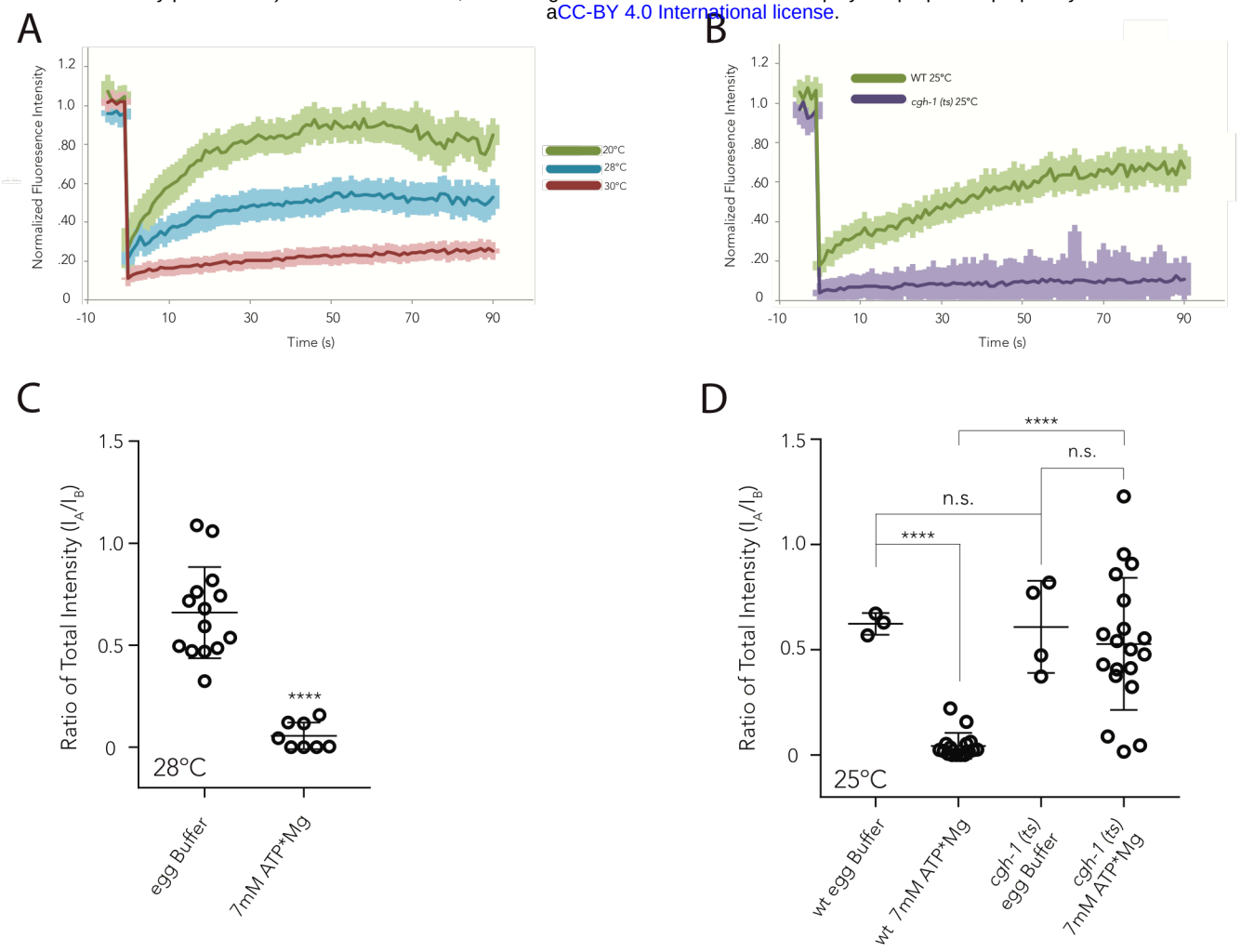

Fig. 3 – Dependence of MEG-3 dynamics on temperature and *cgh-1*^{DDX6} activity

A. MEG::3 dynamics decrease with prolonged incubation at temperatures above the thermal limit. Graph showing MEG-3::GFP fluorescence recovery after photobleaching (FRAP) in embryos (JH3019) raised at 20°C (green) or shifted to 28.3°C for 40 minutes (blue) or 30°C for 2 hours (red). Mean granule fluorescence was measured every second, starting five seconds before bleaching until 90 seconds after bleaching. Values were normalized to initial fluorescence intensity (t = -5 seconds) and plotted as an average of at least 8 granules. Error bars represent mean ± SEM.

B. MEG-3 dynamics decrease in embryos deficient for CGH-1^{DDX6} activity [*cgh-1(ts)*]. Graph showing MEG-3::GFP fluorescence recovery after photobleaching (FRAP) in wild-type embryos (JH3503) and *cgh-1(ts)* embryos (JH3544 and JH3546) raised at 20°C and shifted to 25.3°C for 2 hours. Mean granule fluorescence was measured and plotted as in A.

C. 28°C MEG-3 granules are still sensitive to ATP. Graph showing the fraction of MEG-3 retained in the granular phase after extrusion. MEG-3::GFP embryos (JH3019) were shifted to 28.3°C for 40 minutes before extrusion. Data were obtained and plotted as in Fig. 1B. **** indicates that $p < 0.0001$.

D. *cgh-1(ts)* MEG-3 granules are resistant to dissolution by ATP. Graph showing the fraction of MEG-3 retained in the granular phase after extrusion. Wild-type (JH3503) and *cgh-1(ts)* embryos (JH3544 and JH3546) expressing MEG-3::GFP were shifted to 25.3°C for 2 hours before extrusion. Data were obtained and plotted as in Fig. 1B. n.s indicates that $p > 0.05$, ****$p < 0.0001$. See Fig. S3B for representative photomicrographs.

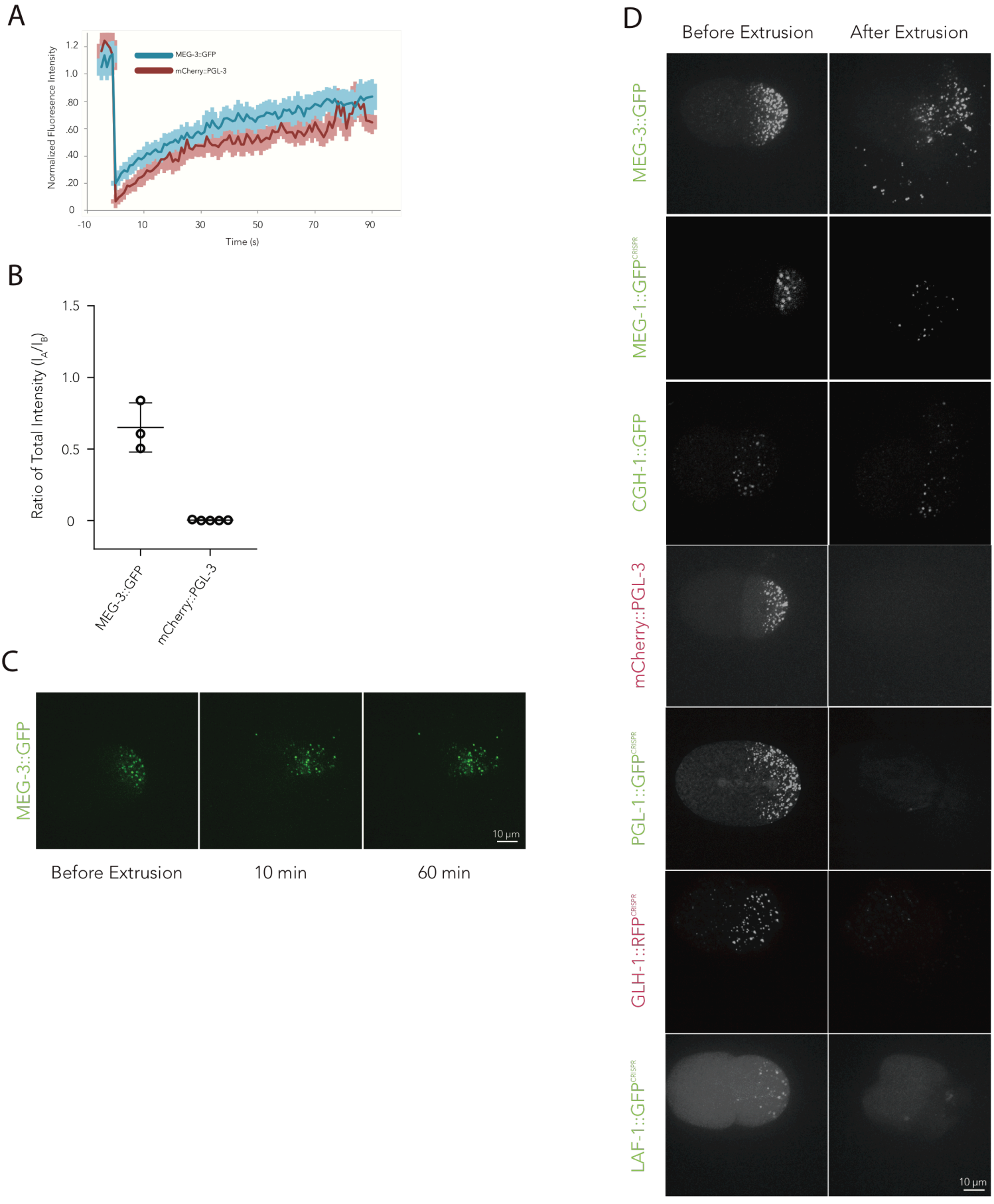

Fig. S1 – P granules contain different phases.

A. MEG:3 and PGL-3 have similar rates of granule/cytoplasmic exchange. Graph showing MEG-3::GFP (blue) and mCherry::PGL-3 (red) fluorescence recovery after photobleaching (FRAP) in embryos (JH3019) raised at 20°C. Mean granule fluorescence was measured every second, starting five seconds before bleaching until 90 seconds after bleaching. Values were normalized to initial fluorescence intensity (t = -5 seconds) and plotted as an average of at least 8 granules. Error bars represent mean ± SEM.

B. MEG-3 and PGL-3 behave differently upon extrusion into egg buffer. Graph showing the fraction of MEG-3::GFP or mCherry::PGL-3 retained in the granular phase after extrusion. Data were acquired using strain JH3019 (Table S1). Data were acquired and plotted as in Fig. 1B. Total fluorescence was measured before laser puncture (I_B) and 60 seconds after laser puncture (I_A). The I_A /I_B ratio is shown for each embryo (circle) extruded into egg buffer as in Fig. 1B. (83 mM NaCl, 33 mM KCl, 1.5 mM $CaCl_2$, 7.5mM $MgCl_2$, 50 mM Hepes pH 7.0). Error bars represent ± SD.

C. Photomicrographs of embryo expressing MEG-3::GFP (JH3503) immediately before, 10 minutes after, and 60 minutes after laser puncture and extrusion of P granules. Scale bar is 10μm.

D. Photomicrographs of embryos expressing MEG-3::GFP (JH3019), MEG-1::GFP (JH3379), CGH-1::GFP (JH1985), mCherry::PGL-3 (JH3019), PGL-1::GFP (JH3269), GLH-1::RFP (JH4007), and LAF-1::GFP (CPB132) before (left) and 60 seconds after (right) laser puncture. Scale bar is 10μm long. MEG-3::GFP and mCherry::PGL-3 images were obtained from the same embryo. Tagged alleles created by genome editing at endogenous loci are indicated by CRISPR superscript. All other images were acquired from transgenic strains (Table S1 for all strains used in this study).

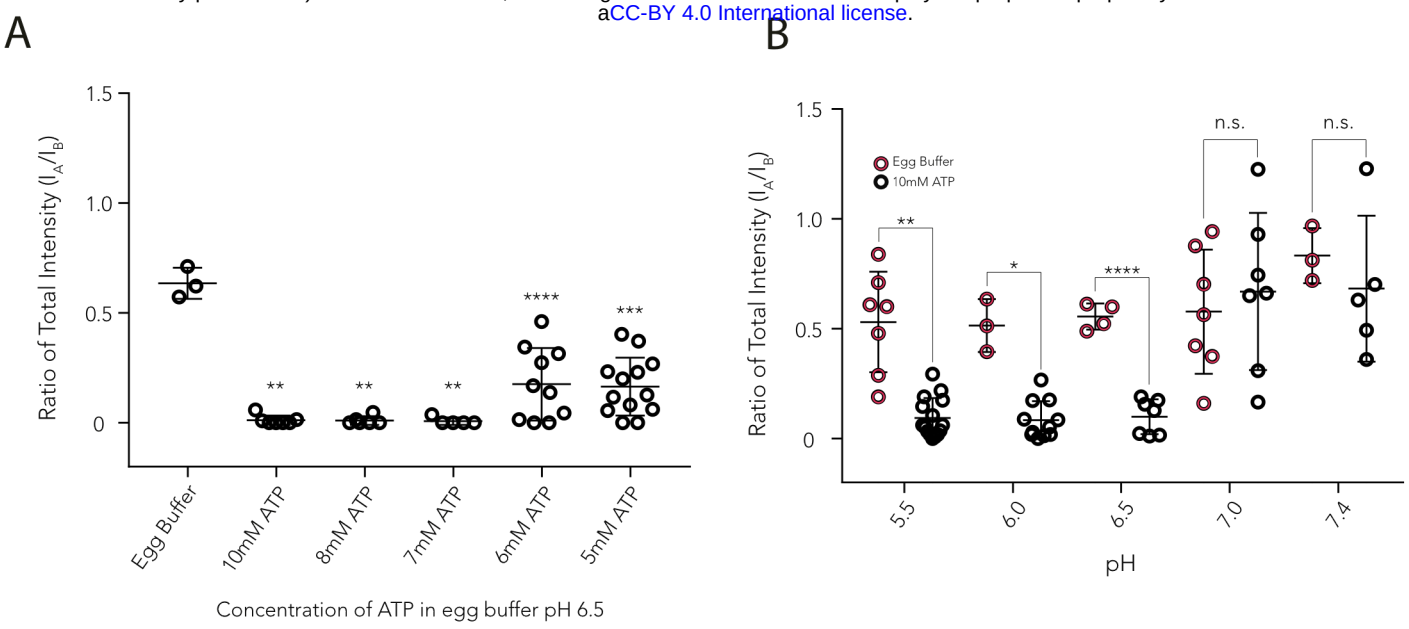

Fig. S2 – Concentration and pH dependence of ATP-mediated P granule dissolution

A. Graph showing the fraction of MEG-3::GFP retained in the granular phase after extrusion into egg buffer containing varying concentrations of ATP*Mg. Data were obtained and plotted as in Fig. 1B. Error bars represent ± SD. X – axis shows the concentration of ATP (pH 6.5) for each group. n.s indicates that $p > 0.05$, **$p < 0.01$, ***$p < 0.001$, ****$p < 0.0001$. Data were acquired using strain JH3503 (Table S1).

B. Graph showing the fraction of MEG-3::GFP retained in the granular phase after extrusion into egg buffer of varying pH with and without 10mM ATP*Mg. Error bars represent ± SD. X – axis shows pH of each pair. n.s indicates that $p > 0.05$, **$p < 0.01$, ***$p < 0.001$, ****$p < 0.0001$. Data were acquired using strain JH3503 (Table S1).

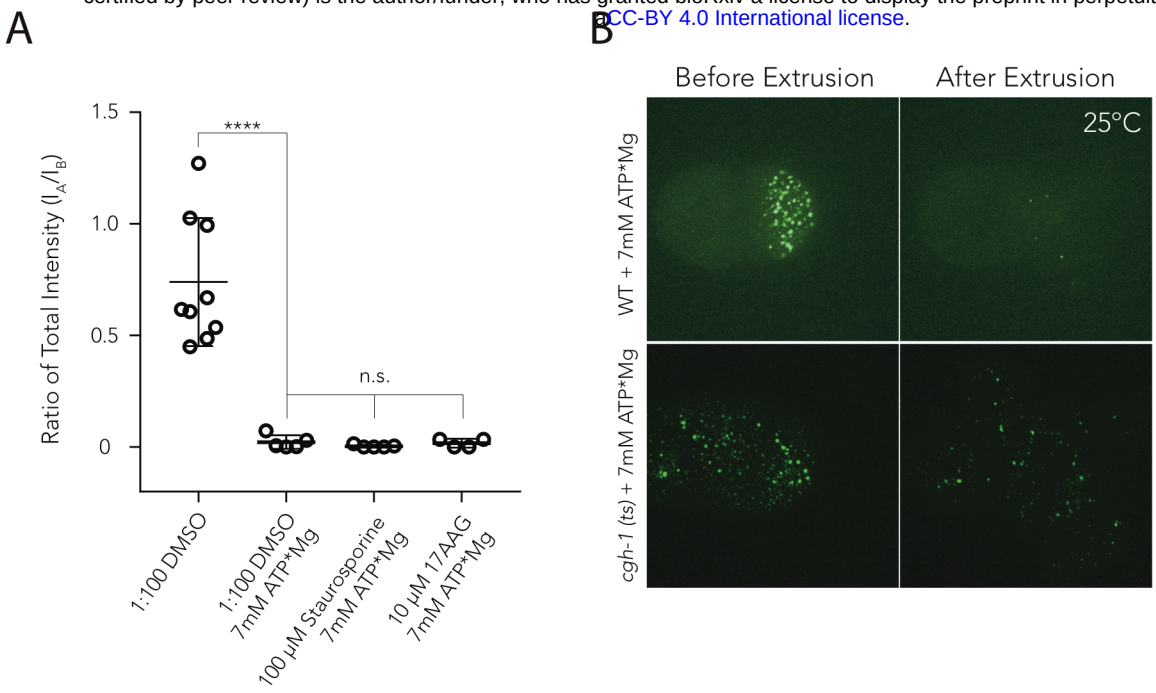

Fig. S3 – ATP-driven dissolution is dependent on CGH-1^{DDX6}

A. Graph showing the fraction of MEG-3::GFP (JH3503) retained in the granular phase after extrusion into egg buffer with DMSO and ATPase inhibitors. X – axis shows the buffer condition for each group. Data were obtained and plotted as in Fig. 1B. Error bars represent ± SD. n.s indicates that $p > 0.05$, *$p < 0.05$, **$p < 0.01$, ***$p < 0.001$, ****$p < 0.0001$.

B. Representative images from experiment shown in Fig. 3D. Photomicrographs of wild-type (JH3503) and *cgh-1(ts)* (JH3546) embryos incubated for 2 hours at 25.3°C and laser punctured to extrude contents into egg buffer supplemented with ATP. Data are quantified in Fig. 3D. Scale bar is 10µm long.

Strain	Genotype	Description	Method	Derived from	Citation
JH3503	*meg-3(ax3054)*	MEG-3::meGFP	CRISPR/Cas9	N2	Smith, Calidas et al. 2016
DG1701	*cgh-1(tn691)*	*cgh-1 ts*	EMS	N2	Yamamoto et al. 2005
JH3544	*meg-3(ax3054); cgh-1(tn691)*	MEG-3::meGFP; *cgh-1 ts*	Cross	JH3503[*meg-3(ax3054)*] xDG1701[*cgh-1(tn691)*]	this study
JH3546	*meg-3(ax3054); cgh-1(tn691)*	MEG-3::meGFP; *cgh-1* ts	Cross	JH3503[*meg-3(ax3054)*] xDG1701[*cgh-1(tn691)*]	this study
JH3019	*meg-3(axIS2076); pgl-3(axIS2077)*	MEG-3::GFP; mCherry::PGL-3	Cross	JH3016[*meg-3(axIS2076)*] xJH2906(*pgl-3(axIS2077)*)	Wang, Smith et al. 2014
JH4007	*glh-1(ax3009)*	GLH-1::tagRFP	CRISPR/Cas9	N2	Paix et al. 2015
JH1985	*cgh-1(axIs1436)*	CGH-1::GFP	transgene	N2	Gallo, Munro et al. 2008
CPB132	*laf-1(ptnIs077)*	LAF-1::GFP	CRISPR/Cas9	N2	Wei, Elbaum-Garfinkle et al. 2017
JH3269	*pgl-1(ax3122)*	PGL-1::GFP	CRISPR/Cas9	N2	Rasoloson, D. Pers. Comm.
JH3379	*meg-1(ax3121)*	MEG-1::GFP	CRISPR/Cas9	N2	Rasoloson, D. Pers. Comm.

Table S1 – Strains used in this study

Two independent MEG-3::GFP; *cgh-1(ts)* lines (JH3544 and JH3546) were obtained and used to generate data for Fig. 3B and Fig. 3D. No differences were noted between the two strains. Only JH3546 was used for Fig. S3B.

Movie 1 – Extrusion of MEG-3::GFP and mCherry::PGL-3 labeled granules in egg buffer

Synchronized maximum projection time-lapse videos showing extrusion of P granules from a *C. elegans* embryo co-expressing MEG-3::GFP (left) and mCherry::PGL-3 (right) into egg buffer. Top left corner shows elapsed time in hrs:mins:secs:msecs. Scale bar is 10μm. Movie was acquired as described in methods using strain JH3019 (Table S1) and is the same embryo depicted in Fig. 1A.

Movie 2 – Extrusion of MEG-3::GFP labeled granules into egg buffer containing ATP

Maximum projection time-lapse video showing extrusion of P granules from a *C. elegans* embryo expressing MEG-3::GFP into egg buffer containing 7mM ATP. Top left corner shows elapsed time, and scale bar is 10μm. Movie was acquired using strain JH3503 (Table S1).

Movie 3 – Extrusion of MEG-3::GFP labeled granules into egg buffer containing ADPnP

Maximum projection time-lapse videos showing extrusion of P granules from a *C. elegans* embryo expressing MEG-3::GFP into egg buffer containing 7mM non-hydrolysable ADPnP. Top left corner shows elapsed time, and scale bar is 10μm. Movie was acquired using strain JH3503 (Table S1).

References

Alberti, S., D. Mateju, L. Mediani and S. Carra (2017). "Granulostasis: Protein Quality Control of RNP Granules." Front Mol Neurosci **10**: 84.

Boke, E., M. Ruer, M. Wuhr, M. Coughlin, R. Lemaitre, S. P. Gygi, S. Alberti, D. Drechsel, A. A. Hyman and T. J. Mitchison (2016). "Amyloid-like Self-Assembly of a Cellular Compartment." Cell **166**(3): 637-650.

Bourgeois, C. F., F. Mortreux and D. Auboeuf (2016). "The multiple functions of RNA helicases as drivers and regulators of gene expression." Nat Rev Mol Cell Biol **17**(7): 426-438.

Brangwynne, C. P., C. R. Eckmann, D. S. Courson, A. Rybarska, C. Hoege, J. Gharakhani, F. Julicher and A. A. Hyman (2009). "Germline P granules are liquid droplets that localize by controlled dissolution/condensation." Science **324**(5935): 1729-1732.

Brangwynne, C. P., T. J. Mitchison and A. A. Hyman (2011). "Active liquid-like behavior of nucleoli determines their size and shape in Xenopus laevis oocytes." Proc Natl Acad Sci U S A **108**(11): 4334-4339.

Brangwynne, C. P., P. Tompa and R. V. Pappu (2015). "Polymer physics of intracellular phase transitions." Nature Physics **11**.

Brenner, S. (1974). "The genetics of Caenorhabditis elegans." Genetics **77**(1): 71-94.

Delgadillo, A. D. (2016). Temperature drives P granule formation in Caenorhabditis elegans. PhD, Max Planck Institute.

Elbaum-Garfinkle, S., Y. Kim, K. Szczepaniak, C. C. Chen, C. R. Eckmann, S. Myong and C. P. Brangwynne (2015). "The disordered P granule protein LAF-1 drives phase separation into droplets with tunable viscosity and dynamics." Proc Natl Acad Sci U S A **112**(23): 7189-7194.

Falahati, H. and E. Wieschaus (2017). "Independent active and thermodynamic processes govern the nucleolus assembly in vivo." Proc Natl Acad Sci U S A **114**(6): 1335-1340.

Hubstenberger, A., C. Cameron, S. L. Noble, S. Keenan and T. C. Evans (2015). "Modifiers of solid RNP granules control normal RNP dynamics and mRNA activity in early development." J Cell Biol **211**(3): 703-716.

Hubstenberger, A., S. L. Noble, C. Cameron and T. C. Evans (2013). "Translation repressors, an RNA helicase, and developmental cues control RNP phase transitions during early development." Dev Cell **27**(2): 161-173.

Humphrey, D., C. Duggan, D. Saha, D. Smith and J. Kas (2002). "Active fluidization of polymer networks through molecular motors." Nature **416**(6879): 413-416.

Hyman, A. A., C. A. Weber and F. Julicher (2014). "Liquid-liquid phase separation in biology." Annu Rev Cell Dev Biol **30**: 39-58.

Jain, S., J. R. Wheeler, R. W. Walters, A. Agrawal, A. Barsic and R. Parker (2016). "ATPase-Modulated Stress Granules Contain a Diverse Proteome and Substructure." Cell **164**(3): 487-498.

Kawasaki, I., A. Amiri, Y. Fan, N. Meyer, S. Dunkelbarger, T. Motohashi, T. Karashima, O. Bossinger and S. Strome (2004). "The PGL family proteins associate with germ granules and function redundantly in Caenorhabditis elegans germline development." Genetics **167**(2): 645-661.

Kedersha, N., S. Chen, N. Gilks, W. Li, I. J. Miller, J. Stahl and P. Anderson (2002). "Evidence that ternary complex (eIF2-GTP-tRNA(i)(Met))-deficient preinitiation complexes are core constituents of mammalian stress granules." Mol Biol Cell **13**(1): 195-210.

Knowles, J. R. (1980). "Enzyme-catalyzed phosphoryl transfer reactions." Annu Rev Biochem **49**: 877-919.

Mildvan, A. S. (1987). "Role of magnesium and other divalent cations in ATP-utilizing enzymes." Magnesium **6**(1): 28-33.

Mugler, C. F., M. Hondele, S. Heinrich, R. Sachdev, P. Vallotton, A. Y. Koek, L. Y. Chan and K. Weis (2016). "ATPase activity of the DEAD-box protein Dhh1 controls processing body formation." Elife **5**.

Needleman, D. and J. Brugues (2014). "Determining physical principles of subcellular organization." Dev Cell **29**(2): 135-138.

Neves, A., C. Busso and P. Gonczy (2015). "Cellular hallmarks reveal restricted aerobic metabolism at thermal limits." Elife **4**: e04810.

Patel, A., L. Malinovska, S. Saha, J. Wang, S. Alberti, Y. Krishnan and A. A. Hyman (2017). "ATP as a biological hydrotrope." Science **356**(6339): 753-756.

Saha, S., Christoph A. Weber, M. Nousch, O. Adame-Arana, C. Hoege, Marco Y. Hein, E. Osborne-Nishimura, J. Mahamid, M. Jahnel, L. Jawerth, A. Pozniakovski, Christian R. Eckmann, F. Jülicher and Anthony A. Hyman (2016). "Polar Positioning of Phase-Separated Liquid Compartments in Cells Regulated by an mRNA Competition Mechanism." Cell.

Shin, Y. and C. P. Brangwynne (2017). "Liquid phase condensation in cell physiology and disease." Science **357**(6357).

Smith, J., D. Calidas, H. Schmidt, T. Lu, D. Rasoloson and G. Seydoux (2016). "Spatial patterning of P granules by RNA-induced phase separation of the intrinsically-disordered protein MEG-3." Elife **5**.

Taylor, J. P., R. H. Brown, Jr. and D. W. Cleveland (2016). "Decoding ALS: from genes to mechanism." Nature **539**(7628): 197-206.

Traut, T. W. (1994). "Physiological concentrations of purines and pyrimidines." Mol Cell Biochem **140**(1): 1-22.

Updike, D. and S. Strome (2010). "P granule assembly and function in Caenorhabditis elegans germ cells." J Androl **31**(1): 53-60.

Updike, D. L., S. J. Hachey, J. Kreher and S. Strome (2011). "P granules extend the nuclear pore complex environment in the C. elegans germ line." J Cell Biol **192**(6): 939-948.

Wang, J. T., J. Smith, B. C. Chen, H. Schmidt, D. Rasoloson, A. Paix, B. G. Lambrus, D. Calidas, E. Betzig and G. Seydoux (2014). "Regulation of RNA granule dynamics by phosphorylation of serine-rich, intrinsically disordered proteins in C. elegans." Elife **3**: e04591.

Wippich, F., B. Bodenmiller, M. G. Trajkovska, S. Wanka, R. Aebersold and L. Pelkmans (2013). "Dual specificity kinase DYRK3 couples stress granule condensation/dissolution to mTORC1 signaling." Cell **152**(4): 791-805.

Wurtz, J. D. and C. F. Lee (2017). "ATP-triggered stress granule formation via phase separation." arXiv: 17.